The application of wave-induced vertical mixing to the KPP scheme

Yonggang Wang[1,2], Fangli Qiao[1,2], Guohong Fang[1,2] and Zexun Wei[1,2]

1. First Institute of Oceanography, State Oceanic Administration, Qingdao, China.
2. Key Laboratory of Marine Science and Numerical Modeling, State Oceanic Administration, Qingdao, China.

Second Revision

April 2010

Corresponding author address:

Professor Fangli Qiao

First Institute of Oceanography, State Oceanic Administration

6 Xian-Xia-Ling Road, Hi-Tech Park, Qingdao

P. R. China, 266061

E-mail: qiaofl@fio.org.cn

Tel: 86-532-88967400

Fax: 86-532-88967400

Abstract

Surface wave-induced vertical mixing is incorporated to modify the K profile parameterization (KPP) scheme. The effects of this modified KPP scheme on a quasi-global oceanic general circulation model are examined by carrying out four test cases. To evaluate simulated upper-layer temperature and surface mixed layer depth (MLD), the model seasonal cycle of temperature and MLD are compared with those from Levitus climatology. In this study, the MLD is defined as the depth that the temperature has changed 0.8°C from the reference depth of 10 m. Statistic analysis shows that test cases with the addition of wave-induced vertical mixing can reduce the root-mean-square difference of upper-layer temperature and increase the correlation with Levitus climatology. Based on comparison with Levitus climatology, the surface wave-induced mixing improves the simulation of MLD in summer time for both hemispheres. Comparing the MLD in different seasons, the wave-induced mixing improves MLD in both hemispheres in summer more than in other seasons. The simulation results are sensitive to weighting coefficients of the wave-induced mixing, suggesting that a preferred weighting coefficient be between 0.1 and 0.3 in the modified KPP scheme.

Key words: wave-induced vertical mixing, KPP, surface mixed layer

1. Introduction

Many ocean modeling studies in literature have focused on understanding the ocean's role in climate change. From this point of view, sea-surface temperature (SST) and ocean mixed layer depth (MLD) are key variables because they directly reveal the interaction between the ocean and atmosphere [Schopf and Loughe 1995; Kara et al., 2003]. In order to predict SST and MLD as accurate as possible, it is necessary to study upper-ocean mixed-layer physics and parameterize related vertical mixing processes [McWilliams, 1996]. A variety of vertical mixing schemes have been developed and tested [e.g., Pacanowski and Philander, 1981; Mellor and Yamada, 1982; Fang and Ichiye, 1983; Price et al., 1986; Chen et al., 1994; Large et al., 1994]. However, the non-breaking surface-wave-induced vertical mixing was not fully considered on these mixing schemes. It is believed that surface waves can enhance mixing in the upper ocean and the wave-induced mixing can improve the simulation of seasonal variations for upper-layer temperature and MLD [Qiao et al., 2004]. The key is how to parameterize mixing processes and to combine the parameterization with existing mixing schemes. By considering the surface wave-induced fluctuation u_{iw} in the Reynolds stress analysis, Qiao et al. [2004, 2008] obtained the expression of non-breaking wave-induced mixing (Bv; following the abbreviated form of Qiao et al. [2004]) and applied Bv to an OGCM with the Mellor-Yamada mixing scheme. Their model results showed much improved simulations of MLD and SST. This kind of wave-induced turbulence unrelated to wave breaking was observed in ingeniously designed laboratory experiments [Babanin and Haus, 2009; Dai et al. 2010]. Numerical experiments have shown that wave-induced vertical mixing plays a key role in climate system [Song et al., 2007; Babanin et al., 2009].

As one of the popular vertical mixing schemes, the K profile parameterization (KPP) scheme [Large et al., 1994] has gained respect as an alternative in deep ocean applications [Large and Gent, 1999; Durski et al., 2004]. In the KPP scheme, turbulence of the oceanic surface boundary layer (OBL) is driven primarily by the surface stress τ_0 and surface buoyancy flux B_f; for the ocean interior, the mixing due to shear instability, internal wave breaking and double diffusion are considered. The OBL turbulence parameterization of KPP is derived from Troen and Mahrt [1986] atmospheric boundary layer (ABL) model with some additional desirable features (see Large et al. [1994] for detailed description). Since the wave-induced mixing is not explicitly considered by the KPP scheme, this study will assess the applicability of adding wave-induced mixing to the KPP scheme.

This paper is organized as follows. Section 2 introduces the model configuration and parameters. Section 3 presents comparisons of simulated SST and MLD with climatological SST and MLD. The conclusions of this study are given in section 4.

2. Model configuration and parameters

Regional Oceanic Modeling System (ROMS) is used in this study. ROMS is a community model shared by a large user group around the world, with applications ranging from studying an entire ocean basin to a coastal sub-region [Haidvogel et al., 2000; Penven et al., 2001; Marchesiello et al., 2003]. It solves incompressible, hydrostatic, primitive equations with free sea surface, horizontal curvilinear coordinates, and a generalized terrain-following vertical coordinate that can be configured to enhance resolutions near sea surface or seafloor. The model domain used for this study includes the quasi-global ocean from 78°S to 65°N with horizontal resolution of $1/2° \times 1/2°$. Twenty terrain-following s-coordinate levels provide high resolution near the surface. The stretching parameter for the vertical grid [Song and Haidvogel, 1994] are $\theta_s = 7$ and $\theta_b = 0.2$. Bathymetry data is derived from the ETOPO5 dataset. The model is forced with surface wind stress, heat and freshwater fluxes, and heat flux sensitivity to SST from the COADS ocean surface monthly climatology [Da Silva et al., 1994]. Cyclic boundary condition is used for the east-west boundaries, and the closed boundary conditions are used for the north and south boundaries. Initial conditions are obtained from

Levitus climatology [Levitus et al., 1994].

The KPP mixing scheme is applied in the model with the common setting. The KPP scheme separates parameterizations of vertical mixing into two distinct parts: one for the ocean interior and the other for the OBL above the boundary layer depth. The formulations of vertical viscosity and diffusivities above h_{sbl} can be expressed as the product of turbulent velocity scales w_M and w_τ, and a non-dimensional vertical shape function $G(\sigma)$. The vertical mixing below the OBL is given by adding the effects of local Richardson number instability due to resolved vertical share, internal wave breaking, and double diffusion.

In addition, the wave-induced mixing Bv is also included, which is simply added to the KPP-derived vertical viscosity and diffusivity. Bv is developed by Qiao et al. [2004] as the following equation,

$$Bv = \alpha \iint_{\vec{k}} E(\vec{k}) \exp(2kz) d\vec{k} \frac{\partial}{\partial z}\left[\iint_{\vec{k}} \omega^2 E(\vec{k}) \exp(2kz) d\vec{k}\right]^{\frac{1}{2}} , \qquad (1)$$

where $E(\vec{k})$ represents wave number spectrum, ω is wave angular frequency, k is the wave number, α is a constant coefficient, and z is the vertical coordinate axis (downward positive) with $z = 0$ at the surface. Bv is expressed as the fuction of wave number spectrum, and can be computed directly by MASNUM (Key Laboratory of Marine Science and Numerical Modeling) wave number spectrum model [Yuan et al., 1991; Yang et al., 2005] because this model is formulated in terms of wave number spectrum. In fact, Bv can also be computed by other wave models, such as the WAM model. But the frequency-directional spectrum should be converted to wave number spectrum firstly,

$$E(\vec{K}) d\vec{K} = F(f, \theta) df d\theta, \qquad (2)$$

then Bv can be integrated by equation (1). The temporal and spatial distributions of Bv used in this study are same as in Qiao et al. [2004].

To discuss the effect of Bv and evaluate its application, several cases are designed in this study. The first case is the control run with the original KPP scheme;

others are sensitive runs with modified KPP scheme. The sensitive runs are designed by the following considerations: (1) Since the wave-induced mixing is not explicitly considered in the KPP scheme, has the wave-induced mixing process been merged into the KPP scheme implicitly? (2) In equation (1), α is an unknown constant coefficient; what value of α is conformable to the KPP scheme? In this study, the sensitive runs are designed with different setting of α. The α can be regarded as weighting coefficients of the wave-induced mixing.

Since Qiao et al. [2004] set $\alpha = 1$ to the Mellor-Yamada scheme and got an improvement for the simulation of temperature in the upper 100 m, we set the same value of α as one of sensitive runs. The model results show some overestimate vertical mixing area by comparing with Levitus climatology [Levitus et al., 1994]. After that we run a series of sensitive runs with different setting of α, and selected 3 typical cases to discuss the application of wave-induced vertical mixing to the KPP scheme in this study. Each value of α for the sensitive runs is listed in Table 1. In this paper, we use CR to indicate control run and SRs to indicate sensitive runs. All cases have been run for 15 years each, and the results in the 15th year are used for analysis.

Figure 1a shows the distribution of h_{sbl} in August derived from CR. It can be seen that h_{sbl} is less than 10 m for the main part of north hemisphere in boreal summer. In austral summer h_{sbl} is less than 10 m nearly in all the southern hemisphere. It is indicated that the notable vertical mixing was trapped within the near surface region in the summer time for both hemispheres in original KPP scheme. Figure 1b is the depth at which K_τ is decreases to 5 cm^2s^{-1} (same as the definition of D_5 in Qiao et al., 2004). The blank area in Figure 1b indicates the vertical diffusivity is less than 5 cm^2s^{-1} at the whole water depth. The distributions of h_{sbl} and the depth of $K_\tau = 5cm^2/s$ show obvious consistency. Comparing with the global distribution of D_5 in August (Figure 2a in Qiao et al., 2004), K_τ derived from original KPP is less significant than Bv in the summer time. Since laboratory experiments by Dai et al. [2010] revealed the existence of turbulence induced by non-breaking surface waves, the original KPP shows some underestimate upper layer vertical diffusivity in summer time. The vertical diffusivity K_τ in CR and SRs are shown in Figure 2. For convenience, the global ocean is separated into three regions, which is defined as Region 1 (RegS; from 60ºS to 20ºS), Region 2 (RegN; from 20ºN to 60ºN), and Region 3 (tropical area from 20ºS to 20ºN). It can be seen that there is not obvious change between CR and SRs in Region 3, because Bv is not comparable with the KPP mixing in the tropics [Qiao, 2004]. For RegS and RegN, however, K_τ displays obvious changes between CR and SRs, especially for cases with high values of α. For boreal and austral winters, the K_τ in the CR is big enough and the K_τ in the SRs does not change its spatial distribution. However, for boreal and austral summers, the effect of Bv is comparable with the original KPP mixing and the upper-layer distribution of K_τ shows distinct change. To demonstrate the effect of Bv, a reference depth is defined, where K_τ = 1 cm^{2}s^{-1}. Table 2 shows the reference depth from the CR and SRs. It is obvious that the reference depth becomes bigger distinctly with increasing α. A deeper reference depth indicates stronger mixing process occurring in the upper layer of the ocean.

3. Model –data comparison

3.1 Comparison method

To evaluate the applicability of Bv, several statistical methods are used to compare the model outputs and Levitus climatology. The monthly means of temperature and MLD are considered in this study.

Following the statistical methods of Kara et al. [2003], X_i (i =1, 2, … n) is a set of reference values (i.e., Levitus temperature), and Y_i (i =1, 2, …, n) is a set of estimates (i.e., simulated temperature by the CR and SRs). $\overline{X}$ ($\overline{Y}$) and σ_X (σ_Y) are the mean and standard deviations of the reference (estimates) values, respectively. We evaluate time series of modeled monthly-mean temperature from January to December at each grid point over the model domain. Thus, n is 12 in this study. Following the work of Murphy [1988] and Stewart [1990], the statistical relationship between Levitus temperature (X) and simulated temperature (Y) can be expressed as follows:

$$ME_i = Y_i - X_i \tag{2}$$

$$RMS = \left[\frac{1}{n} \sum_{i=1}^{n} (Y_i - X_i)^2 \right]^{1/2} \tag{3}$$

$$R = \frac{1}{n} \sum_{i=1}^{n} \frac{(X_i - \overline{X})(Y_i - \overline{Y})}{(\sigma_X \sigma_Y)} \tag{4}$$

$$SS = R^2 - \left[R - (\sigma_Y \sigma_X) \right]^2 - \left[(\overline{Y} - \overline{X}) / \sigma_X \right]^2 \tag{5}$$

where ME_i is the bias of the i^{th} month, RMS is the root-mean-square (RMS) difference, R is the correlation coefficient, and SS is the skill score. For 12 monthly-mean temperature at each grid point over the global ocean, the R value must be at least ± 0.53 for it to be statistically different from R=0 based on *t*-test at the 95% confidence level [Neter et al., 1988].

The SS in Equation (5) is computed by accounting for two biases, termed conditional and unconditional biases [Kara et al. 2003]. Unconditional bias (also called systematic bias, B_{UC}) is a measure of the difference between the means of simulated temperature, while the conditional bias (B_C) is a measure of the relative amplitude of the variability in the two datasets [Murphy 1992]. The SS based on RMS difference can be defined as $SS = 1 - RMS^2 / \sigma_X^2$ and this is mathematically equivalent to Equation (5).The SS is 1.0 for perfectly simulated temperature [e.g., Murphy and Daan 1985], and positive skill is usually considered to represent a minimal level of acceptable performance. Note that the correlation coefficient squared is equal to SS only when both conditional and unconditional biases are zero. Because the two biases are never negative, the correlation can be considered as a measure of ‘‘potential’’ skill, that is, a skill that can be obtained by eliminating biases from the model. Using the preceding statistical measures, we will perform model–data comparisons for temperature next.

3.2 Comparison for upper-layer temperature

Comparison of the seasonal variation for upper layer temperature anomalies at 50 ° N, 145° W was shown in Figure 3a. For the CR, the isotherm was trapped winthin the upper 20 m layer. The seasonal variation of SR[1] shows reasonable fit with Levitus data. To valid the Levitus data, the seasonal variation of upper layer temperature observed at Ocean Station Papa is shown in Figure 3b. These two data show essential agreement except Leitus data are smoother.

To avoid any contamination of other processes from surface boundary conditions, the 10-m depth temperature of the CR and SRs are compared with Levitus climatology. February and August are selected as representatives, because these two months are the summer time for each hemisphere, when large proportion of upper-layer vertical mixing is contributed by Bv. Figure 4 shows the comparison of ME_2 and ME_8 (the subscript i represents the i^{th} month) for the CR and SRs at 10-m depth. In RegS, ME_2 of the CR shows much discrepancy south of 45°S. However, ME_2 of the SRs seems better. This improvement is mainly due to incorporating Bv to the vertical mixing scheme. At the austral summer time, the surface layer is stable stratification with low salinity and high temperature in RegS, accompanying with small h_{sbl} (less than 10 m) in original KPP scheme. The depth of K_τ = 1 cm^{2}s^{-1} is about 20 m in CR (Figure 2) south of 45°S. The warm water was trapped at the upper 40 m, and therefore overestimated temperature exists south of 45°S at 10 m depth in CR. After incorporating Bv to the vertical mixing scheme, the K_τ is big enough to mix the upper water with lower water, and improve the thermal structure for the Southern Ocean. In RegN, ME_2 show much discrepancy in the northwest Atlantic. It is mainly due to the close boundary condition at 65°N. In the

Northeast Pacific, an overestimated area appears gradually with increasing the effect of Bv (i.e. increasing the value of α). The vertical profile of the regional average (180°E-130°W, 40°N-60°N, see Figure 5) temperature for the Northeast Pacific shows a maximum temperature existed at the depth about 100 m. As the ocean loses heat in North Pacific in February, the stronger vertical mixing can compensate the losing heat from lower water and leads to higher temperature in upper layers.

The upper-layer temperature differences in August are shown in Figure 4b. In RegS, there are not any difference between CR and SRs. In RegN, a large underestimated area exists north of 30°N in the Northwest Pacific. This underestimated area was reduced in the SR with α =0.1, but increases again with increasing the value of α . In boreal summer, the h_{sbl} is quite shallow (less than 5 m, see Figure 1a) in RegN, corresponding with a weak vertical mixing in CR especially between 40°N-50°N (Figure 2b) where fits with the underestimated area in CR. The depth of K_τ = 1 cm^{2}s^{-1} is less than 10 m in CR, therefore underestimated temperature exists at 10 m. After incorporating Bv to the vertical mixing scheme with α =0.1, the upper mixed layer becomes deeper than CR (about 20-30 m), and the underestimated area was reduced. With increasing the value of α , the upper mixed layer becomes so deep that the upper layer temperature was underestimated by the excess heat transmitting from upper layer to lower layer.

Figure 6 exhibits the *RMS* for the CR and SRs. Same as the upper-layer temperature, the significantly improved areas are the Southern Ocean and the Northwest Pacific. Table 3 lists the regional average *RMS* for the CR and SRs. It can be seen that SR with α =0.1 is the most favorable one; it reduces the RMS of RegS from 1.09°C to 0.89°C, and the RMS of RegN from 1.0°C to 0.85°C.

After comparing with the upper-layer temperature (at 10-m depth), the average correlation coefficients (Equation (4)) for RegS and RegN are calculated for the upper 100-m depth, which shows the critical level for confidence level of 95% by *t*-test (Figure 7). Each correlation coefficient of the SRs is remarkable higher than correlation coefficient of CR in the full upper 100-m depth, which exhibits that Bv can improve the simulated temperature structure for the entire upper layer. According to compare the upper-layer temperature with Levitus data, the higher correlation coefficient of SRs is mainly due to the improvement of the vertical structure of summer time temperature. In RegS (Figure 7a), correlation coefficient of CR reaches the critical level at about 70 m. That means under this depth, the simulated seasonal variation of the temperature is not significantly correlated with Levitus data. However, after considering the effect of Bv, the critical depth can reach about 100 m. Thinking over the difference value of α for Bv, there are some differences between them: the higher value of α the more significant correlation there is for the depth greater than 50 m. In RegN (Figure 7b), all of the correlation coefficients of the SRs are higher than correlation coefficient of CR at the full upper 100-m depth as well. Different with RegS, there is no obvious difference between SRs. The top 100-m average of correlation coefficient for CR and SRs are listed in Table 3. It can be seen that SRs improve the correlation coefficient of RegS from 0.68 to greater than 0.8, and for RegN from 0.82 to ~0.9.

The regional averages of the statistical measures mentioned in 3.1 (SS, B_C, and B_{UC}) are calculated for RegS and RegN and shown in Figure 8. In RegS, the SS of SRs is more desirable than SS of CR except in the surface area (0-20 m). In Figure 8a, a turning point exists near 35-m depth. Up to this depth, the lower value of α, the better SS and the better model performance. On the contrary, below this depth, the higher value of α exhibits better skill for simulating the temperature. Figure 8b shows the B_C values in RegS. Since B_C is a measure of the relative amplitude of temperature between the simulated and Levitus data, the decrease of B_C indicates that Bv can improve the simulation of temperature for seasonal variation. Figure 8c shows the values of B_{UC} in RegS. The B_{UC} values of SRs are better than those of CR below 15-m depth. Since B_{UC} is a measure of the difference between the means of temperature between the simulated and Levitus data, the change of B_{UC} indicates that Bv can improve the simulation of temperature for annual-mean values. The SS in RegN shows more applicable than that in RegS. In Figure 8d, most depths show great improvement for the skill of simulating temperature. Figure 8e shows the B_C values in

RegN. The change of B_C indicates that Bv can improve the simulation of temperature for seasonal variation. Figure 5f shows the B_{UC} values in RegN. The B_{UC} values of SRs are better than those of CR except in near-surface areas. The change of B_{UC} indicates that Bv can improve the simulation of temperature for annual-mean values in RegN.

3.3 Comparison for MLD

In this section, monthly-mean MLD values obtained from the CR and SRs are compared to those obtained from Levitus climatology. Owing to the fact that the MLD is very deep in winter time for both hemispheres, only the summer time MLD is shown. In this study, the MLD is defined as the depth that the temperature has changed 0.8°C from the reference depth of 10 m.

Figure 9a shows the distribution of MLD for the Levitus data, the CR and SRs for RegS in February; Fig. 6b shows the distribution of MLD for RegN in August. For the summer time in the Southern Hemisphere (Figure 9a), the MLD of CR is shallower than the Levitus between 20°S and 40°S. After incorporating Bv to the mixing scheme, the MLD of SRs with α =0.1 and 0.3 are more comparable to that of Levitus than the MLD of CR is. However, the SR with α =1.0 shows some overestimated MLD in the Southern Ocean. For the summer time of the Northern Hemisphere (Figure 9b), the MLD of CR is shallower than the Levitus north of 25°N. After considering Bv in the mixing scheme, both the values and distributions of the MLD of SR with α =0.1 is improved significantly. For big values of α , however, an overestimated tendency is obvious.

4. Summary and conclusions

In this study, the wave-induced mixing is incorporated into the KPP scheme to study its impact on upper-ocean processes. One CR and 3 SRs with different effect of the wave-induced mixing are carried out. Comparison of the model results shows the following. The modified KPP scheme can improve the simulation of upper-layer temperature and MLD in mid- and high latitudes for RegS and RegN. Thinking over the effect of different value of α for the wave-induced mixing, the reasonable value of α should be between 0.1 and 0.3 in the KPP scheme.

This study focuses on the application of the wave-induced mixing in the KPP scheme in an OGCM. In a coastal area or a regional basin, the applicable of the wave-induced mixing in the KPP scheme needs further study. Some related work has been done on the Mellor-Yamada scheme, giving some reasonable results [Qiao et al., 2004b; Qiao et al., 2006; Xia et al., 2006].

Acknowledgement:

This research was supported by the National Natural Science Foundation of China through grants 40730842 and 40606006. The authors wish to thank the reviewers for their constructive comments.

References

Babanin, A. V., B. K. Haus (2009), On the Existence of Water Turbulence Induced by Non-Breaking Surface Waves, *J Physical Oceanography*, DOI: 10.1175/2009JPO4202.1.

Babanin, A. V., A. Ganopolski, and W. R.C. Phillips (2009), Wave-induced upper-ocean mixing in a climate model of intermediate complexity, *Ocean Modelling*, 189-197. doi:10.1016/j.ocemod.2009.04.003.

Chen, D., A. J. Busalacchi, and L. M. Rothstein (1994), The roles of vertical mixing, solar radiation, and wind stress in a model simulation of the sea surface temperature seasonal cycle in the tropical Pacific Ocean, *J Geophys Res*, 99:20 345-20 359.

Dai, D. J., F. Qiao, W. Sulisz, L. Han, and A. Babanin (2010), An experiment on the non-breaking surface-wave-induced vertical mixing, *J. Phys. Oceanogr (submitted, under second revision).*

da Silva, A. M., C. C. Young, and S. Levitus (1994), Algorithms and Procedures. Vol. 1, Atlas of Surface Marine Data 1994, NOAA Atlas NESDIS 6, 83 pp.

Durski, S. M., S. M. Glenn, and D. B. Haidvogel (2004), Vertical mixing schemes in the coastal ocean: Comparison of the level 2.5 Mellor-Yamada scheme with an enhanced version of the K profile parameterization, *J. Geophys. Res.*, 109, C01015, doi:10.1029/2002JC001702.

Fang, G., and T. Ichiye (1983), On the vertical structure of tidal currents in a homogeneous sea, *Geophys. J. Internatioanl*, 73, 65– 82.

Haidvogel, D. B., H. Arango, K. Hedstrom, A. Beckmann, P. Malanotte-Rizzoli, and S.

Shchepetkin (2000), Model evaluation experiments in the North Atlantic Basin: simulations in non-linear terrain-following coordinates, *Dyn. Atmos. Oceans,* 32, 239–282.

Kara, A. B, Alan J. Wallcraft, and H. E. Hurlburt (2003), Climatological SST and MLD predictions from a global layered ocean model with an embedded mixed layer, *J. Atmos. Oceanic Technol*, 20, 1616– 1632.

Large, W. G., J. C. McWilliams, and S. C. Doney (1994), Oceanic vertical mixing: A review and a model with a nonlocal boundary layer parameterization, *Rev. Geophys.*, **32,** 363–403.

Large, W. G., G. Danabasoglu, S.C. Doney, and J.C. McWilliams (1997), Sensitivity to surface forcing and boundary layer mixing in a global ocean model: Annual-mean climatology, *J. Phys. Oceanogr.* **27**, 2418–2447.

Large, W. G., and P. R. Gent (1999), Validation of vertical mixing in an equatorial ocean model using large eddy simulations with observations, *J. Phys. Oceanogr*., 29, 449– 464.

Levitus, S. and T. Boyer (1994), World Ocean Atlas. Washington D C: NOAA, 117.

Marchesiello, P., J. C. McWilliams, A. Shchepetkin (2003), Equilibrium structure and dynamics of the California Current System, *J. Phys. Ocean.* 33, 753–783.

McWilliams, J. C. (1996), Modeling the oceanic general circulation. *Annu. Rev. Fluid Mech.*, **28,** 215–248.

Mellor, G. L., and T. Yamada (1982), Development of a turbulence closure model for geophysical fluid problems, *Rev. Geophys.*, 20, 851– 875.

Murphy, A. H. (1988), Skill scores based on the mean square error and their relationships to the correlation coefficient, *Mon. Weather Rev*., 116, 2417–2424.

Murphy, A. H. (1992), Climatology, persistence, and their linear combination as standards of reference in skill scores, *Wea. Forecasting,* **7,** 692–698.

Murphy, A. H., and H. Daan (1985), Forecast evaluation. *Probability, Statistics, and Decision Making in the Atmospheric Sciences,* A. H. Murphy and R. W. Katz, Eds., Westview Press, 379–437.

Neter, J., W. Wasserman, and G. A. Whitmore (1988), *Applied Statistics.* Allyn and Bacon, 1006 pp.

Pacanowski, R. G., and S. G. H. Philander (1981), Parameterization of vertical mixing in numerical models of the tropical oceans, *J. Phys. Oceanogr*., 11, 1443–1451.

Penven, P., C. Roy, G. B. Brundrit, A. Colin de Verdière, P. Fréon, A. S. Johnson, J. R. E. Lutjeharms, and F. A. Shillington (2001), A regional hydrodynamic model of upwelling in the southern Benguela, *South African Journal of Science*, 97: 472-475.

Price, J. F., R. F. Weller, and R. Pinkel (1986), Diurnal cycling: Observations and models of the upper ocean response to diurnal heating, cooling and wind mixing, *J. Geophys. Res.*, 91, 8411 – 8427.

Qiao, F., Y. Yuan, Y. Yang, Q. Zheng, C. Xia, and J. Ma (2004), Wave induced mixing in the upper ocean: Distribution and application to a global ocean circulation model, *Geophys. Res. Lett.*, 31, L11303, doi:10.1029/2004GL019824.

Qiao, F., J. Ma, Y. Yang, and Y. Yuan (2004), Simulation of the temperature and salinity along 36°N in the Yellow Sea with a wave-current coupled model, *Journal of the Korean Society of Oceanography*, 2004,39(1):35-45.

Qiao, F., J. Ma, C. Xia, Y. Yang, and Y. Yuan (2006), Influence of the surface wave-induced and tidal mixing on vertical temperature structure of the Yellow and East China Seas in summer, *Progress in Natural Science*，16（7）：739-746.

Qiao, F., Y. Yang, C. Xia, and Y. Yuan (2008), The role of surface waves in the ocean mixed layer, *Acta Oceanologica Sinica*, 27(3):30-37.

Schopf, P. S., and A. Loughe (1995), A reduced-gravity isopycnal ocean model: Hindcasts of El Niño. *Mon. Wea. Rev.*, **123,** 2839–2863.

Song, Z., F. Qiao, Y. Yang, and Y. Yuan (2007), An improvement of the too cold tongue in the tropical Pacific with the development of an ocean-wave-atmosphere coupled numerical model, *Progress in Natural Science*， 17(5):576-583.

Song, Y. T., and D. Haidvogel (1994), A semi-implicit ocean circullation model using a generalized topography following coordinate system, *J. Comp. Phys.* 115, 228–248.

Stewart, T. R. (1990), A decomposition of the correlation coefficient and its use in analyzing forecasting skill. *Wea. Forecasting,* **5,** 661–666.

Troen, I. B., and L. Mahrt (1986), A simple model for the atmospheric boundary layer: Sensitivity to evaporation, *Boundary Layer Meteorol.*, 37, 129– 148.

Xia, C., F. Qiao, Y. Yang, J. Ma, and Y. Yuan (2006), Three-dimensional structure of the summertime circulation in the Yellow Sea from a wave-tide-circulation coupled model, *J. Geophys. Res.*, *111*, C11S03, doi:10.1029/2005JC003218.

Yang, Y, F Qiao, W Zhao, Y Teng, and Y Yuan (2005) MASNUM ocean wave numerical model in spherical coordinates and its application. *Acta Oceanol Sin* 22(2): 1-7

Yuan, Y, Z Pan, F Hua, L Sun (1991) LAGDF-WAM numerical wave model. *Acta Oceanol Sin* 10: 483– 488

Table Captions

Table 1 Weighting coefficient of wave-induced mixing for the CR and SRs.

Table 2 Reference depth (m) in RegS and RegN for the CR and SRs. The reference depth is defined as the depth of K_τ = 1 cm^{2}s^{-1}.

Table 3 the regional average of RMS for the CR and SRs at 10 m, the regional and vertical (top 100m) average of correlation coefficient for the CR and SRs.

Figure Captions

Figure 1a The distribution of h_{sbl} in August derived from CR.

Figure 1b the depth of $K_\tau = 5cm^2/s$. The blank area indicates the vertical diffusivity less than 5 cm^{2}s^{-1} at the whole water depth.

Figure 2a Zonally averaged distribution of vertical diffusivity K_τ for the CR and SRs in February. Contour interval is 2 cm^{2}s^{-1} from 1 to 5 cm^{2}s^{-1}, 5 cm^{2}s^{-1} from 5 to 10 cm^{2}s^{-1}, 20 cm^{2}s^{-1} from 10 to 100 cm^{2}s^{-1} and 500 cm^{2}s^{-1} from 500 to 2000 cm^{2}s^{-1}.

Figure 2b Same as Figure 2a, except for August.

Figure 3a Comparison of the seasonal variation for upper layer temperature anomalies at 50° N, 145° W.

Figure 3b Comparison of the seasonal variation of upper layer temperature between Levitus data and Ocean Station Papa data.

Figure 4a The mean bias in February between model and Levitus climatology at 10 m. Positive values for model warmer than Levitus.

Figure 4b Same as Fig. 4a, except for August.

Figure 5 Comparison of RMS between the CR and SRs at 10 m depth.

Figure 6 The vertical profile of the regional average (180°E-130°W, 40°N-60°N) temperature and salinity in February.

Figure 7a the regional average over RegS of correlation coefficient for temperature between the simulated and Levitus vs depth from 0 to 100 m. Values above the dashed line at 0.53 are statistically significant.

Figure 7b Same as Figure 7a, except for RegN.

Figure 8 The regional average of skill score, conditional bias, and unconditional bias for temperature between the simulated and Levitus data vs depth from 0 to 100 m. (a) the regional average of skill score over RegS, (b) the regional average of conditional bias over RegS, (c) the regional average of unconditional bias over RegS, (d) the regional average of skill score over RegN, (e) the regional average of conditional bias over RegN, (f) the regional average of unconditional bias over RegN.

Figure 9a Distributions of MLD of RegS in February. The MLD is defined as the depth at which the temperature decreased 0.8°C from the reference depth of 10 m

Figure 9b Same as Fig. 7a, except for RegN in August.

Table 1

Run cases	CR	SR^1	SR^3	SR^f
weighting coefficient α	—	0.1	0.3	1

Table 2

Run cases	CR	SR^1	SR^3	SR^f
RegS in February	15.2	18.4	26.0	37.0
RegN in August	23.3	29.8	36.1	44.3

Table 3

		CR	SR^1	SR^3	SR^f
RMS	RegS	1.09	0.89	0.92	0.97
	RegN	1.00	0.85	0.91	1.04
correlation coefficient	RegS	0.68	0.80	0.83	0.83
	RegN	0.82	0.90	0.91	0.89

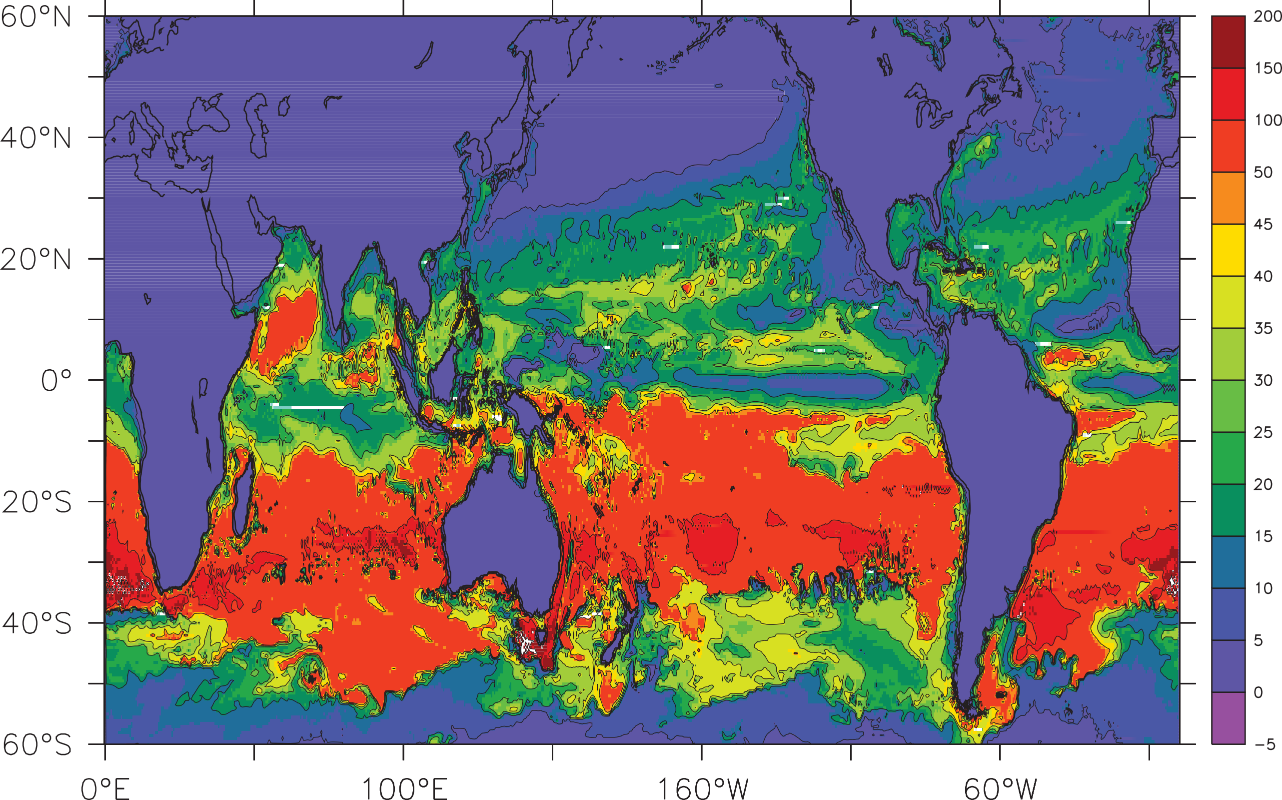
60°N
40°N
20°N
0°
20°S
40°S
60°S
0°E
100°E
160°W
60°W
200
150
100
50
45
40
35
30
25
20
15
10
5
0
−5

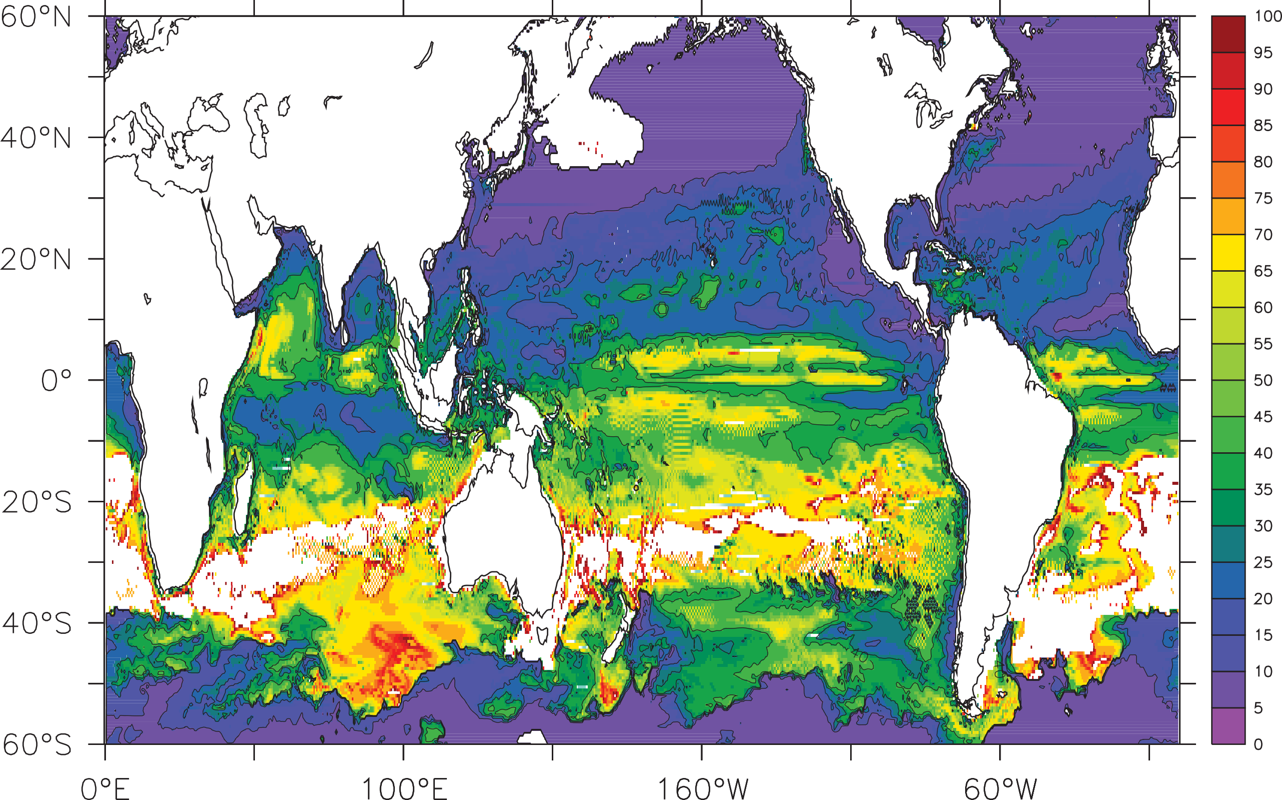

60°N
40°N
20°N
0°
20°S
40°S
60°S
0°E
100°E
160°W
60°W
100
95
90
85
80
75
70
65
60
55
50
45
40
35
30
25
20
15
10
5
0

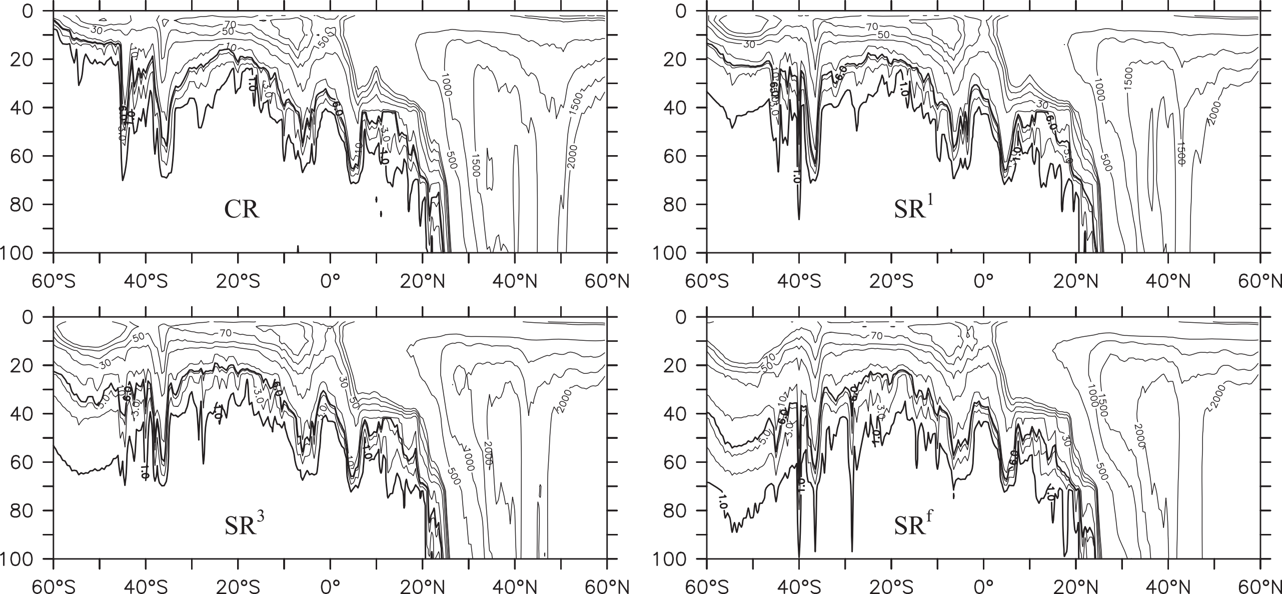
CR
SR1
SR3
SRf
0
20
40
60
80
100
60°S
40°S
20°S
0°
20°N
40°N
60°N
30
50
70
10
1.0
3.0
5.0
6.0
500
1000
1500
2000

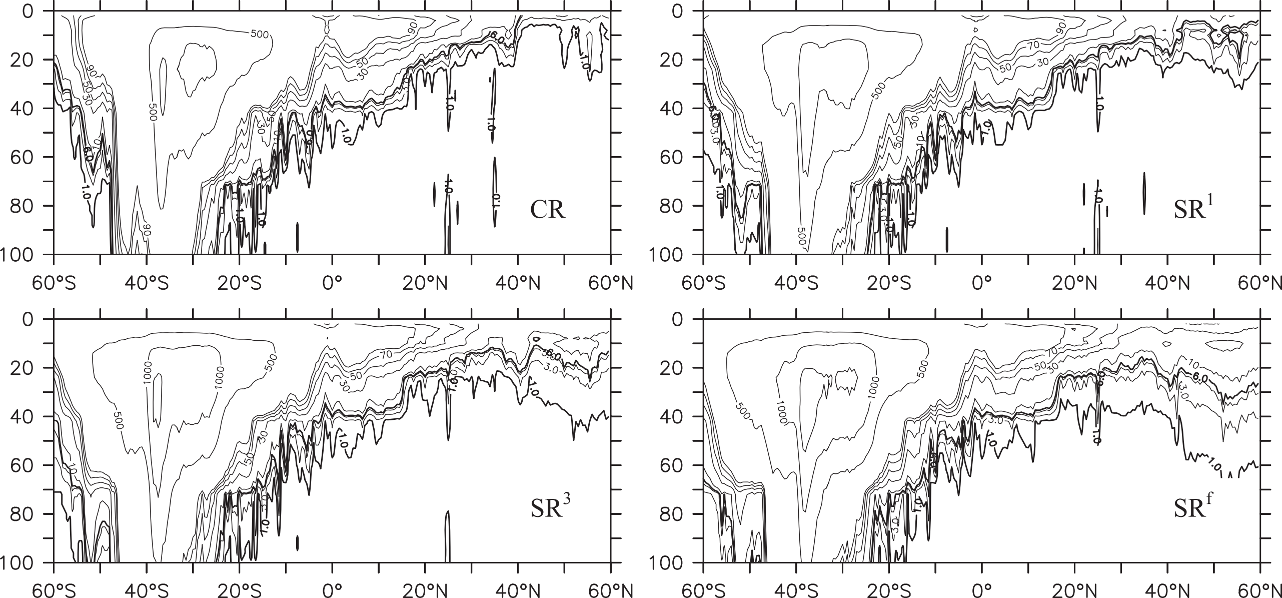
CR
SR1
SR3
SRf
60°S
40°S
20°S
0°
20°N
40°N
60°N
0
20
40
60
80
100

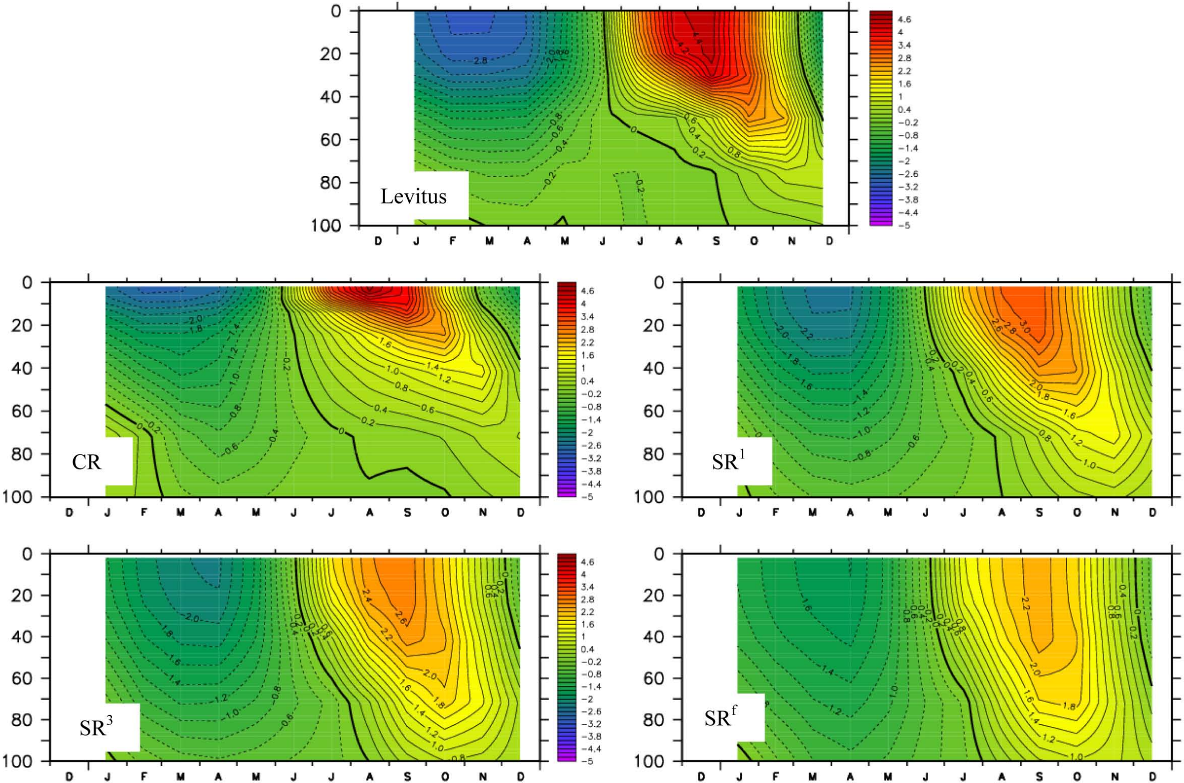
Levitus
CR
SR1
SR3
SRf
0
20
40
60
80
100
D J F M A M J J A S O N D
4.6
4
3.4
2.8
2.2
1.6
1
0.4
−0.2
−0.8
−1.4
−2
−2.6
−3.2
−3.8
−4.4
−5

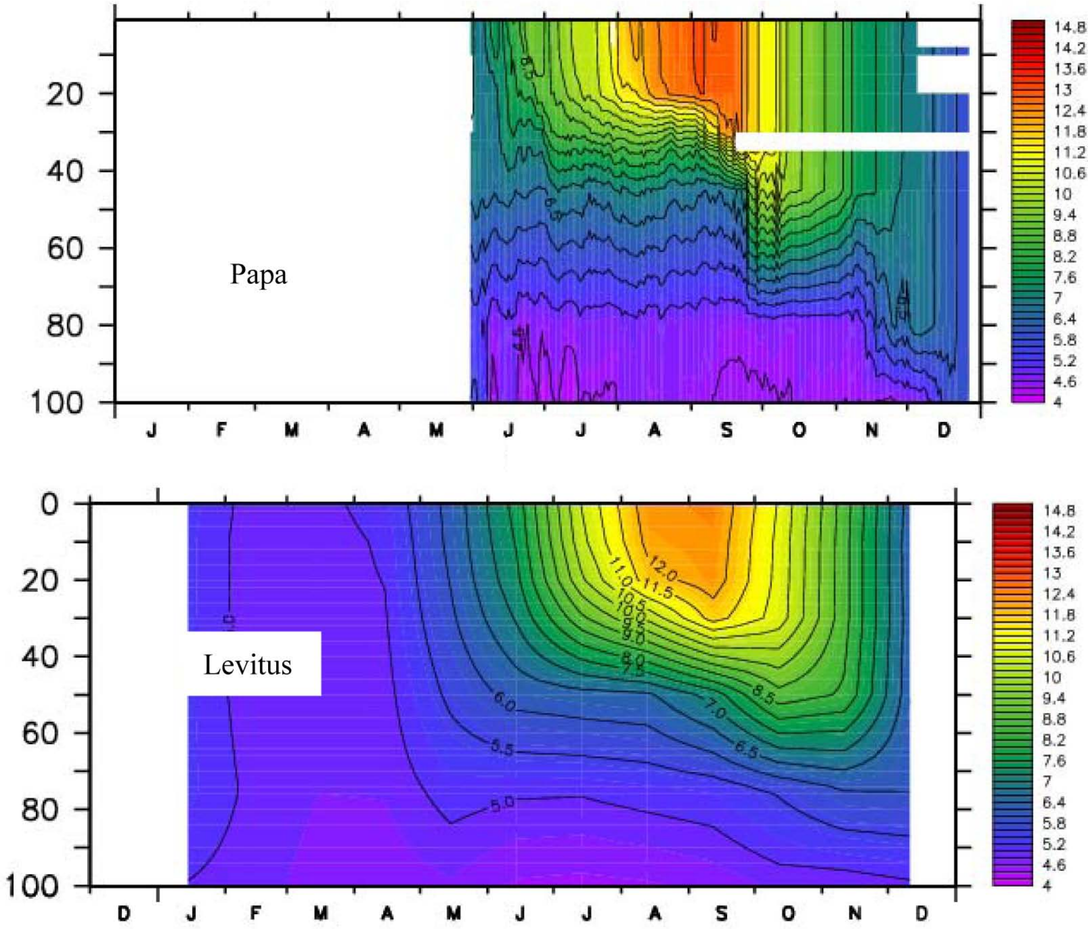

Papa
20
40
60
80
100
J F M A M J J A S O N D
14.8
14.2
13.6
13
12.4
11.8
11.2
10.6
10
9.4
8.8
8.2
7.6
7
6.4
5.8
5.2
4.6
4
Levitus
0
20
40
60
80
100
D J F M A M J J A S O N D
12.0
11.5
11.0
10.5
8.0
7.5
8.5
7.0
6.5
6.0
5.5
5.0
14.8
14.2
13.6
13
12.4
11.8
11.2
10.6
10
9.4
8.8
8.2
7.6
7
6.4
5.8
5.2
4.6
4

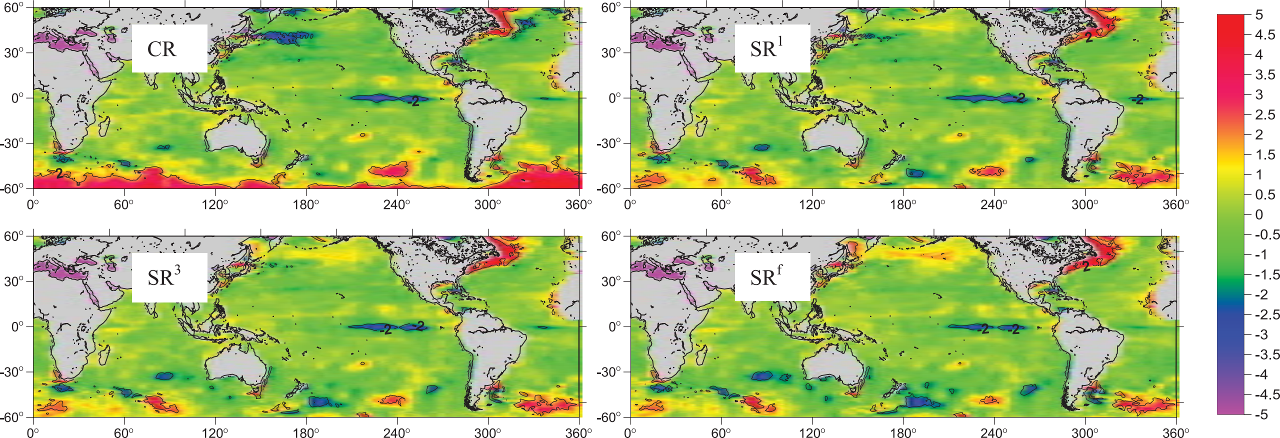
CR
SR1
SR3
SRf
60°
30°
0°
-30°
-60°
0°
60°
120°
180°
240°
300°
360°
-2
2
5
4.5
4
3.5
3
2.5
2
1.5
1
0.5
0
-0.5
-1
-1.5
-2
-2.5
-3
-3.5
-4
-4.5
-5

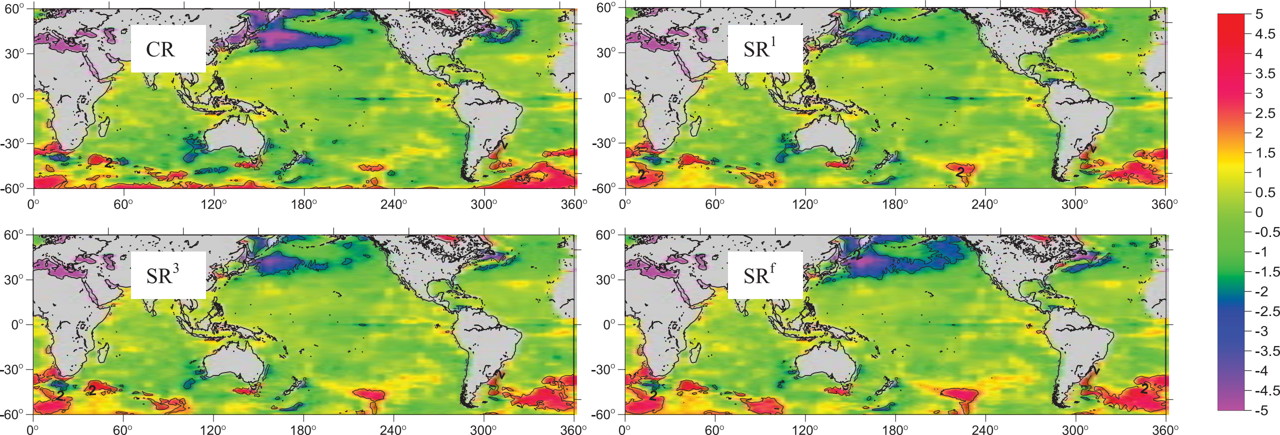
CR
SR1
SR3
SRf
60°
30°
0°
-30°
-60°
0°
60°
120°
180°
240°
300°
360°
5
4.5
4
3.5
3
2.5
2
1.5
1
0.5
0
-0.5
-1
-1.5
-2
-2.5
-3
-3.5
-4
-4.5
-5

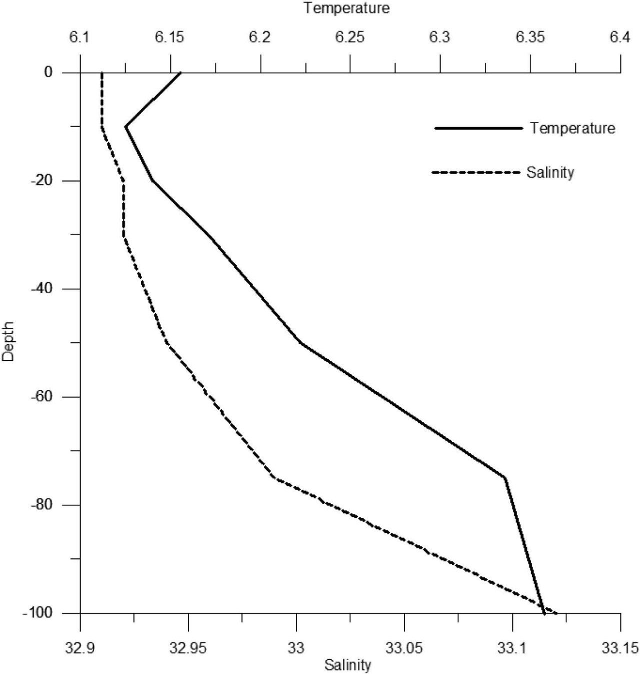

Temperature
6.1
6.15
6.2
6.25
6.3
6.35
6.4
0
-20
-40
-60
-80
-100
Depth
Temperature
Salinity
32.9
32.95
33
33.05
33.1
33.15
Salinity

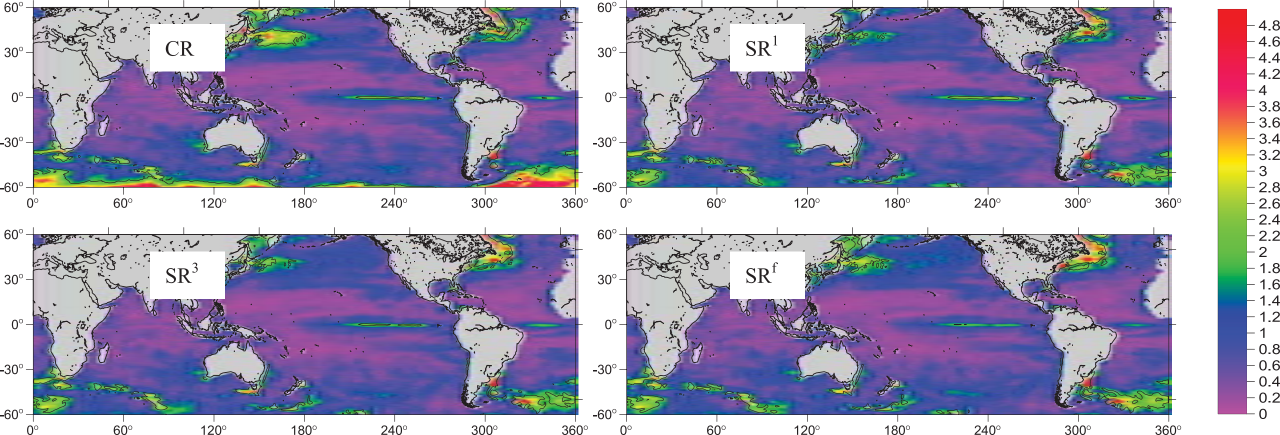
CR
SR1
SR3
SRf
60°
30°
0°
-30°
-60°
0°
60°
120°
180°
240°
300°
360°
4.8
4.6
4.4
4.2
4
3.8
3.6
3.4
3.2
3
2.8
2.6
2.4
2.2
2
1.8
1.6
1.4
1.2
1
0.8
0.6
0.4
0.2
0

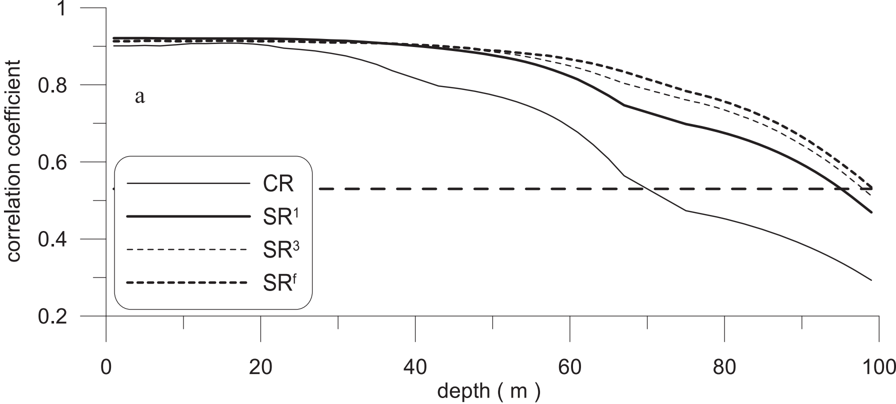
a
correlation coefficient
depth (m)
CR
SR1
SR3
SRf
0.2
0.4
0.6
0.8
1
0
20
40
60
80
100

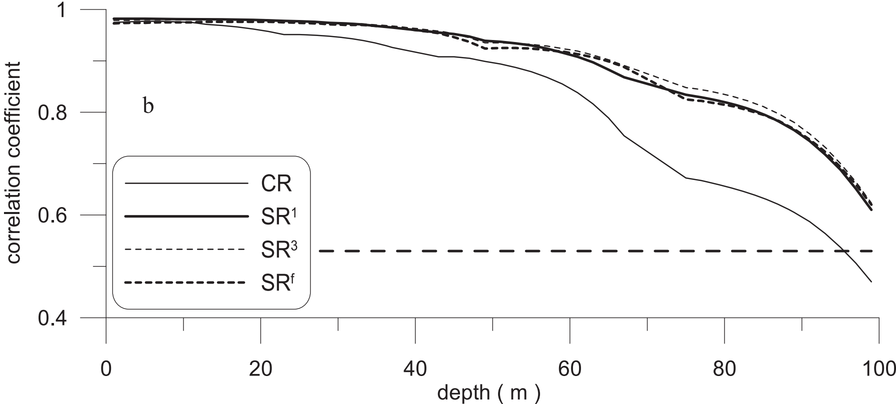
b
correlation coefficient
depth (m)
CR
SR1
SR3
SRf
0.4
0.6
0.8
1
0
20
40
60
80
100

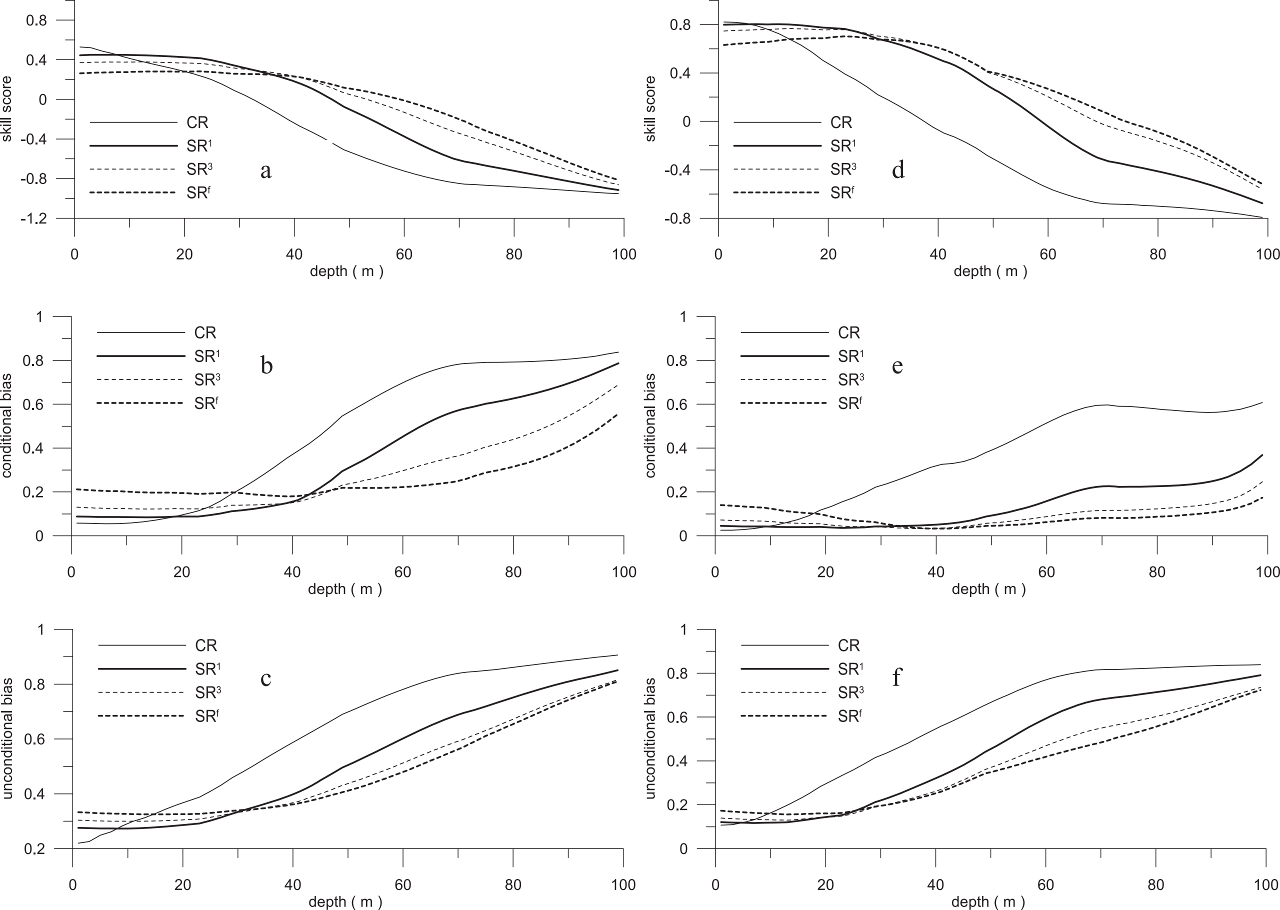
a
b
c
d
e
f
CR
SR1
SR3
SRf
skill score
conditional bias
unconditional bias
depth (m)

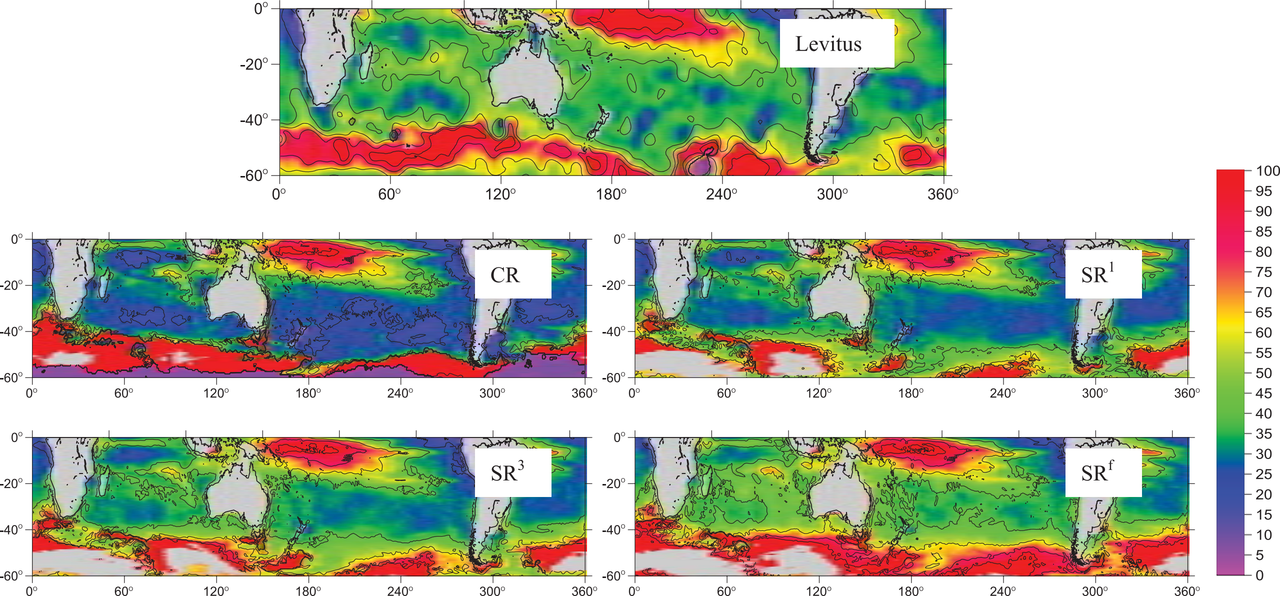
Levitus
CR
SR1
SR3
SRf
0°
-20°
-40°
-60°
0°
60°
120°
180°
240°
300°
360°
100
95
90
85
80
75
70
65
60
55
50
45
40
35
30
25
20
15
10
5
0

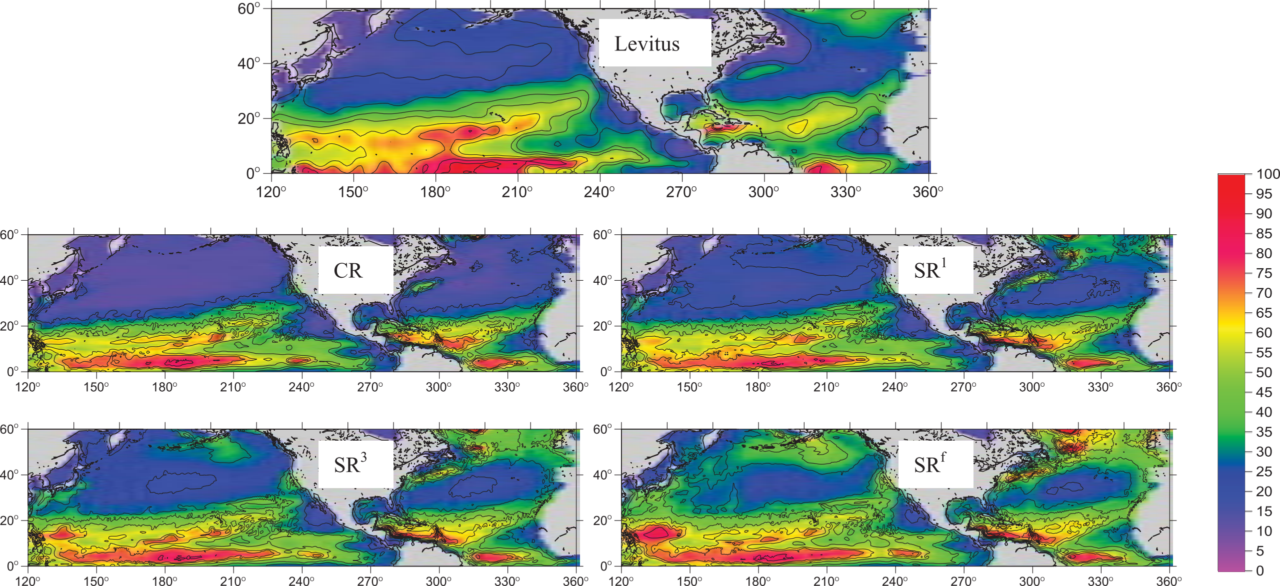
Levitus
CR
SR1
SR3
SRf
60°
40°
20°
0°
120°
150°
180°
210°
240°
270°
300°
330°
360°
100
95
90
85
80
75
70
65
60
55
50
45
40
35
30
25
20
15
10
5
0